applied optics

Analysis of thermo-optic effect-based refractive index dynamic modulation in microspherical resonator

Yue Wang,[1,2] Quan-Long Wang,[1,2] Song Zhou,[1,2] Jun-Feng Wu,[1] and Yi-Hui Wu[1,*]

[1]State Key Laboratory of Applied Optics, Changchun Institute of Optics, Fine Mechanics and Physics, Chinese Academy of Sciences, Changchun 130033, China
[2]University of Chinese Academy of Sciences, Beijing 100039, China
*Corresponding author: yihuiwu@ciomp.ac.cn

Received 15 June 2015; revised 29 August 2015; accepted 2 September 2015; posted 2 September 2015 (Doc. ID 242948); published 25 September 2015

The thermo-optic effect has been utilized to modulate the refractive index dynamically within a whispering gallery mode resonator. Modulation with a large tuning range is mostly performed for mode locking and dynamic control of the optical path at a modulation frequency as low as several hertz, while high-frequency modulation up to megahertz is mainly exploited in optical switching devices with small tuning range. Here, we introduce the response functions theoretically to describe the dynamic response of temperature changes in the mode volume and the resonator body, respectively. This result is verified experimentally in silica microspherical resonators. The dependence of the tuning range on the modulation frequency is achieved. This knowledge could pave the way toward more practical control of refractive index in microresonators.

OCIS codes: (140.4780) Optical resonators; (170.4090) Modulation techniques; (190.4870) Photothermal effects; (230.0230) Optical devices.

http://dx.doi.org/10.1364/AO.54.008363

1. INTRODUCTION

The combined ultrahigh quality factor (Q) and ultrasmall mode volume (V) of a whispering gallery mode (WGM) resonator make it a practical optical element to investigate light–matter interaction [1–5]. Thermo-optic effect induced refractive index (RI) change, which shifts the resonance of a resonator, universally exists due to the high rate of Q/V even at a low power level [6–8]. This effect offers a practical approach to modulate the RI of a WGM resonator. When studying nonlinear frequency conversion and tunable optical functional elements [9–12], a large tuning range is preferable, which can only be completed at modulation frequency as low as several hertz. Furthermore, thermo-optic effect-based all-optical devices, like optical switching and optical diode, have also been intensively exploited due to their fast response, where a small resonance shift is sufficient and high speed is required [13–16]. Recently, this effect has been used to modulate the RI both in the mode volume and the resonator body of a WGM resonator. By simply scanning the pump wavelength back and forth on the blue side of a resonance [17,18], the RI of the resonator as well as its resonance frequency will track this scan. It is the scan-induced dynamic temperature response in the resonator that tunes the RI.

For a typical WGM resonator, mode volume is a small fraction inside the resonator body, and the thermal relaxation time is several orders of magnitude smaller in the mode volume. Thus, the two parts experience different temperature changes during scanning [7]. And their dynamic temperature responses rely on the modulation frequency [18]. To achieve more practical modulation of the RI, quantitative analysis about the dynamic response of temperature change is required. Here, we introduced the response functions to describe theoretically the dynamic responses of temperature changes in the mode volume and the resonator body, respectively. The dependence of tuning range on the modulation frequency was achieved. The theoretical results were verified experimentally in silica microspherical resonators. This knowledge could pave the way toward more practical control of RI in WGM microresonators and present instructions for thermo-optic effect-based optical switching devices.

2. MODEL AND DISCUSSION

Thermo-optic effect-based RI modulation is related to the thermal dissipation process in the microresonators. As the thermal conductivity of the resonator body is far larger than that of the surroundings (usually air), heat generated by photon

absorption dissipates to the resonator body, and then to the surroundings. To investigate the dynamic responses of temperature changes in the mode volume and the resonator body theoretically, we introduced the models in [7,19]:

$$\dot{\alpha} = \left[i\Delta_0 - ig_{\text{th}}(\Delta T_1 + \Delta T_2) - \frac{\kappa}{2}\right]\alpha + \sqrt{\kappa_{\text{ex}}}s. \quad (1)$$

$$\Delta \dot{T}_1 = -\frac{k_1}{C_{p1}}\Delta T_1 + |\alpha|^2\frac{\Gamma_{\text{abs}}}{C_{p1}}. \quad (2)$$

$$\Delta \dot{T}_2 = \frac{k_1}{C_{p2}}\Delta T_1 - \frac{k_2}{C_{p2}}\Delta T_2. \quad (3)$$

Equations (1)–(3) describe the amplitude of the intracavity field and temperature changes in the mode volume and resonator body, respectively. α is the normalized amplitude of the optical field in the microresonator, $|s|^2$ is the input field power, and $\Delta_0 = \omega_l - \omega_0$ is the laser frequency (ω_l) detuning from the cavity resonance (ω_0). κ (κ_{ex}) is the loaded (external) cavity optical energy decay rate, $g_{\text{th}} = (-dn/dT) \times (\omega_0/n)$ is the thermo-optic tuning coefficient. $\Delta T_1(\Delta T_2)$ is the temperature difference between the mode volume and the resonator body (the body and the surroundings), $k_1(k_2)$ is the thermal conductivity between the mode volume and the body (between the body and the surroundings), and $C_{p1}(C_{p2})$ is the thermal capacity of the mode volume (the body). Γ_{abs} is the component of optical energy dissipation due to material absorption.

Solving Eqs. (1)–(3) can give a typical thermal bistability curve, which includes a stable warm equilibrium and an unstable warm equilibrium between the absorbed and dissipated heat [7]. The stable warm equilibrium is self-stable, i.e., the resonance trends to shift toward such a direction that the frequency shift induced by the fluctuations of the pump frequency or intensity is compensated. In our experiment, RI modulation is enabled by artificially modulating the pump frequency around a stable equilibrium position. When the pump light frequency shift is small, the above equations were solved using a perturbation approach [19]. The RI change can be quantified by the resonance frequency shift. To relate the RI change to the frequency shift of pump light, we built up the response function. It is defined as the ratio of the resonance frequency shift to the pump light frequency shift (see Appendix A for more details):

$$K_1(\Omega) = \left(1 + \frac{k_1/C_{p2}}{k_2/C_{p2} + i\Omega}\right) \cdot \frac{\beta \cdot P_{\text{in}}}{i\Omega + \frac{k_1}{C_{p1}} + \beta \cdot P_{\text{in}} + \beta \cdot P_{\text{in}}\frac{k_1}{C_{p2}}/\left(\frac{k_2}{C_{p2}} + i\Omega\right)}. \quad (4)$$

$$K_2(\Omega) = \frac{k_1/C_{p2}}{k_2/C_{p2} + i\Omega} \cdot \frac{\beta \cdot P_{\text{in}}}{i\Omega + \frac{k_1}{C_{p1}} + \beta \cdot P_{\text{in}} + \beta \cdot P_{\text{in}}\frac{k_1}{C_{p2}}/\left(\frac{k_2}{C_{p2}} + i\Omega\right)}. \quad (5)$$

In Eqs. (4) and (5), $K_1(\Omega)$ and $K_2(\Omega)$ denote resonance frequency shift response functions of the mode volume and the resonator body, respectively. Ω denotes the modulation frequency, P_{in}, equaled to $|s|^2$, is the input power, and parameter β mirrors the dependence on the Q-factor and frequency detuning between the pump light wavelength and the cavity resonance:

$$\beta = g_{\text{th}}\frac{\Gamma_{\text{abs}}}{C_{p1}}\frac{2\kappa_{\text{ex}}(\Delta_0 - g_{\text{th}}\Delta T_0)}{\left[(\Delta_0 - g_{\text{th}}\Delta T_0)^2 + \frac{\kappa^2}{4}\right]^2}. \quad (6)$$

In addition, we introduced the laser-microresonator relative frequency response function to reflect their relative frequency detuning, $R_i(\Omega) = 1 - K_i(\Omega)(i = 1, 2)$. A smaller $R(\Omega)$ means that the resonance frequency can track the pump light shift more tightly.

The dependence of $K(\Omega)$ and $R(\Omega)$ on the modulation frequency is presented in Fig. 1(a). From this figure we can see that the dynamic tuning range decreases as the modulation frequency increases. Because the response of temperature change depends upon the progress of the thermal dissipation during each modulation period, the increase of modulation frequency leads to the decrease of heat generated, as well as the time left for the heat to dissipate in each period. This feature can be figured out through $R(\Omega)$. As thermal dissipation progress can be quantified by the thermal relaxation rate (shown as the two dotted lines in Fig. 1), when the modulation frequency draws close to the thermal relaxation rate, the incomplete dissipation leads to an increase in $R(\Omega)$, i.e., the resonance frequency cannot track the pump light wavelength shift tightly any longer. Thus, the amplitude of $K(\Omega)$ decreases as the modulation frequency increases.

Meanwhile, the mode volume and the resonator body respond differently to the increase of modulation frequency. The amplitude of the ratio of $K_1(\Omega)$ to $K_2(\Omega)$ reflects the difference of temperature changes between the two parts:

$$\left|\frac{K_1(\Omega)}{K_2(\Omega)}\right| = \left|\frac{k_1 + k_2 + i\Omega C_{p2}}{k_1}\right|. \quad (7)$$

For the thermal conductivity of the mode volume k_1 is far larger than that of the resonator body k_2, at low modulation frequency, the ratio is close to unity. It means that heat generated in the mode volume has sufficient time to dissipate to the body and the environments, i.e., the two parts experience the same temperature change. As the modulation frequency increases, the amplitude of $K_2(\Omega)$ decreases in a large scale, while that of $K_1(\Omega)$ only experiences slight decrease. As a consequence, at high modulation frequencies only the mode volume can be effectively tuned, while at low modulation frequencies the entire microresonator can be tuned simultaneously.

Moreover, we find that the modulation bandwidth of the two parts react differently to the input power, as shown in Fig. 1(b). The modulation bandwidth of the mode volume is extended at high input power, while that of the body is insensitive to the power. Because at higher input power the temperature in the mode volume experiences larger change, the resonance frequency can track the pump wavelength more tightly. Parameter β behaves similarly as P_{in} in determining the bandwidth. Locating the pump wavelength near the bottom of the resonance or exciting a high Q-factor resonance can enhance parameter β as well as the bandwidth.

Finally, the entire microresonator can be tuned in a large tuning range at low modulation frequency. High input power and high-Q resonance selected can enhance the tuning range to be as large as a free spectrum range [20]. Because the tuning system responds linearly to the shift of the pump wavelength [18], we can infer that the tuning range will decrease when the modulation frequency draws close to the slow thermal relaxation rate.

3. EXPERIMENT RESULTS AND DISCUSSION

To illustrate the conclusions experimentally, we used the experimental setup in Fig. 2(a). Microspherical WGM resonators were fabricated by fusing the end of a half-tapered fiber with a fiber fusion splicer, obtained by heating and stretching a standard telecom fiber (radius 125 μm). Using different numbers of arc discharges, spheres with radii ranging from 30 to 103 μm were produced. The pump light from a tunable laser evanescently excited the WGMs in a silica microsphere through a tapered fiber. The output energy was evaluated using a photodetector (125 MHz) connected to an oscilloscope. Precise control of the scanning range enables locking of the pump wavelength on the blue side of a resonance when it is thermally broadened. By scanning the pump light wavelength using a digital function generator at varied velocities, i.e., modulating at different frequencies, the dynamic response of the transmission was obtained. The modulation frequency used in this method is limited to 1 kHz by the tunable laser. By performing Fourier transform of the transmission waveform as shown in Fig. 2(c), the modulation amplitude corresponding to each modulation frequency was derived. And it was related to the theoretical result by the response function defined as $S(\Omega)$ [19],

$$S(\Omega) = P_{\text{in}} \cdot h(\Omega) \cdot R(\Omega), \tag{8}$$

where $h(\Omega)$ is the cavity response function [10]:

$$h(\Omega) = \frac{2i\kappa_e\Delta_0(-\kappa+\kappa_e+i\Omega)}{\left[\Delta_0^2+\left(\frac{\kappa}{2}\right)^2\right]\left[\Delta_0^2+\left(\frac{\kappa-2i\Omega}{2}\right)^2\right]}. \tag{9}$$

Figure 3 presents the experimental and theoretical results of $R(\Omega)$ at two different input powers. The theoretical predictions at high modulation frequencies can be verified by the experimental data in [19,21]. The good agreement confirms the aforementioned first three conclusions. This knowledge lays the foundation for tunable optical switching devices, which can be performed by locating the probe light in the mode volume of the pump light. Enhancing the input power can extend the modulation bandwidth and tuning the primary frequency detuning between the laser and resonance can adjust the

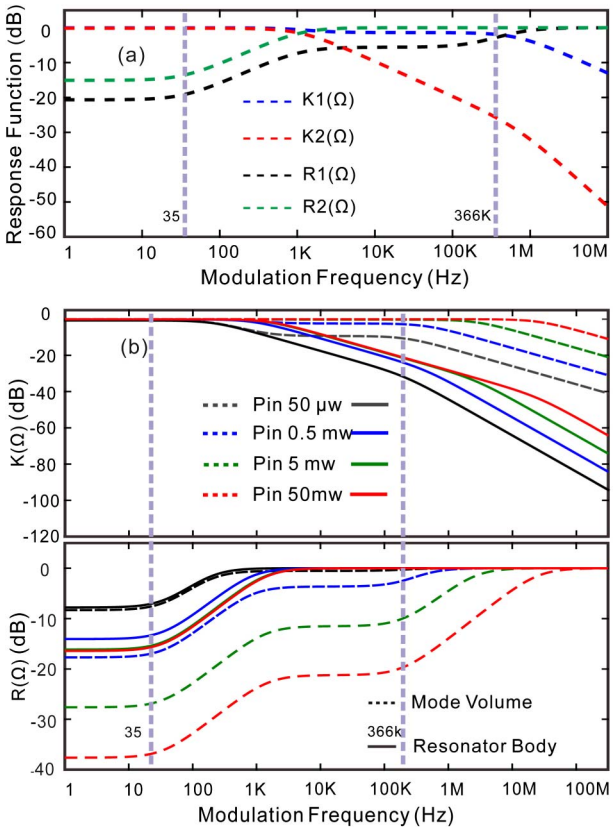

Fig. 1. (a) Resonance frequency shift response functions $K(\Omega)$ and the laser-microresonator relative frequency response functions $R(\Omega)$, respectively. The two dotted lines denote the slow thermal relaxation rate (left) and the fast thermal relaxation rate (right). The input power is 0.1 mW. (b) Dependence of the response functions on the input power. The parameters used here are $K_2/C_{p2} = 35$ Hz, $K_1/C_{p1} = 366$ kHz, $\beta = 5$ MHz/mW.

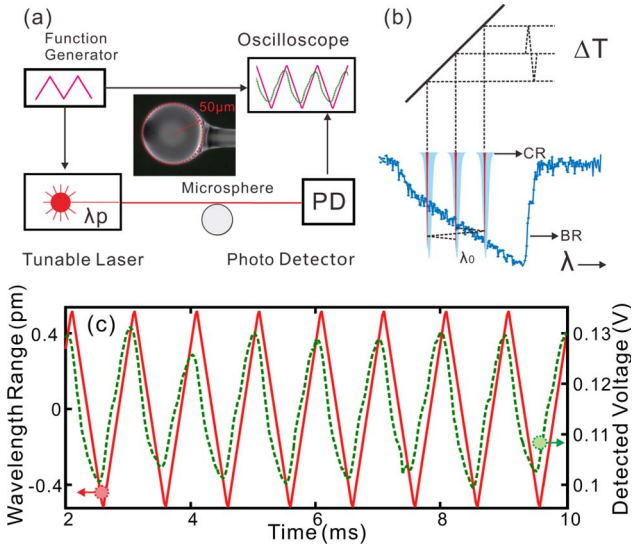

Fig. 2. (a) Experimental setup, the inset is an optical picture of a microsphere with 50 μm radius. (b) Schematic mechanism of RI modulation demonstrated in the experiment. Modulation is performed by scanning the pump light (red peak, linewidth is 200 kHz) within a thermally broadened resonance (blue line) and the blue peak denotes the resonance (linewidth is several megahertz) at each moment. CR, cold resonance; BR, broadened resonance. (c) Experimental transmission waveform achieved via the oscilloscope at modulation frequency of 1000 Hz. The red line and blue dotted line denote the pump light wavelength and detected voltage in the photodetector, i.e., transmission waveform, respectively. The scanning range of the pump wavelength is set to be 1.05 pm, small enough to be considered as perturbation. Normally, the pump wavelength and the transmission waveform are in opposite phase; the mismatch in this plot is attributed to the phase delay that results from the tunable laser.

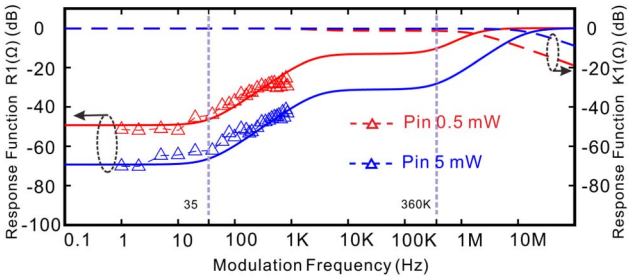

Fig. 3. Theoretical and experimental results of laser-microresonator relative frequency response function $R_1(\Omega)$ (theory in solid line, experiment in triangle) and resonance frequency shift response function $K_1(\Omega)$ (dotted line) at two different input powers. The radius of microsphere used here is 37 μm. The fitting parameters in this plot are $K_2/C_{p2} = 35$ Hz and $K_1/C_{p1} = 360$ kHz.

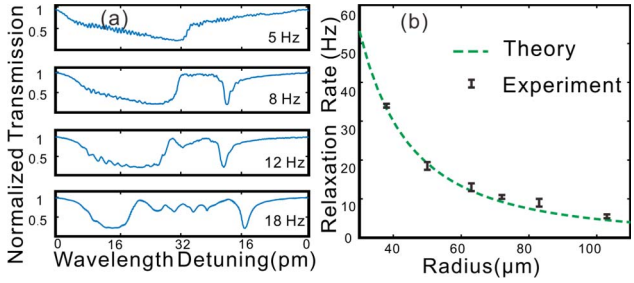

Fig. 4. (a) The dependence of maximum tuning range on the modulation frequency. The radius of the sphere is 50 μm, and its slow thermal relaxation rate is estimated to be 19 Hz. The dip in the transmission spectrum during the down-scan process is the cold resonance corresponding to the broadened resonance in the up-scan process. (b) Experimental corner frequency and theoretical thermal relaxation rate [20]. Error bars are standard deviations from the measurements of two different resonance modes.

working wavelength. Furthermore, different modes have diverse mode patterns and mode volumes. Qualitatively, high-order azimuthal mode has extended nonlocalized mode distribution and larger mode volume than the fundamental mode, which results in a faster thermal dissipation process, i.e., higher relaxation rate. A high-order mode is thus believed to broaden the modulation bandwidth.

The parameters used in the fittings are listed in Table 1. It is not easy to exactly estimate the thermal constants of the mode volume. In general, its thermal relaxation rate is estimated by $\gamma_1 = D/(\delta R)^2$, where D is the temperature conductivity and δR is the effective thickness of the mode near the microsphere surface [6], and can be estimated using the finite element method. Furthermore, the relaxation rate of the resonator body is calculated by $\gamma_2 = K_2/C_2$ [20]. Here, $K_2 = 4\pi R\kappa_2$ is thermal conductivity of the resonator body, and $C_2 = 4/3\pi R^3\rho C_{sp}$ is its thermal capacity, where R is the radius of the sphere, κ_2 is the thermal conductivity between the resonator and air, ρ and C_{sp} are density and specific heat capacity (per mass) of silica, respectively. As for the coupling parameters, it is noted that κ_{ex} and $\Delta_0 - g_{th}\Delta T_0$ are both typically of the same order as κ, about 10^7 for a mode with $Q(10^6$–$10^7)$ around 1550 nm. And material absorption-induced dissipation rate $\Gamma_{abs} = \omega/Q_{abs} = c \times \alpha/n_{eff}$, where the absorption rate α for a standard telecom fiber is 4.6×10^{-5} m^{-1}, n_{eff} is the effective RI, and c is the light speed in vacuum. According to Eq. (6), parameter β is thus of the order of 10^9 [Hz/W]. The fittings were achieved by adjusting these parameters in reasonable ranges to ensure the best agreement with the experimental data.

To illustrate experimentally the response characteristic of modulation in a large range, we produced microspheres with different radii and selected two resonances of each microsphere. Under constant input power, we attained the maximum tuning range for each resonance at low modulation frequency. Then we increased the frequency gradually to the slow thermal relaxation rate. The tuning range, i.e., the thermal broadening, was found to decrease by a half, as presented in Fig. 4(a). The experimental corner frequency where the broadening range halves for each sphere is well around the theoretical slow thermal relaxation rate, as shown in Fig. 4(b). This means that below this modulation frequency, we can achieve the maximum tuning range of RI modulation in the entire microresonator. This presents instructions for WGM microresonator experiments and tunable optical elements.

Moreover, the thermal relaxation rates are well estimated by fitting the experimental data to the function $R(\Omega)$. These parameters are difficult to evaluate in theory because they are interfered with many factors, e.g., geometry of the microresonator and the excited mode [6]. This knowledge is practical for WGM microresonators applied in integrated optical devices.

4. CONCLUSIONS

To summarize, the dynamic response characteristics of temperature change in the mode volume and the microresonator body are illustrated theoretically when performing thermo-optical effect-based RI modulation. The tuning range starts to decrease as the modulation draws close to the thermal relaxation rate. Moreover, the bandwidth of high-frequency modulation in the mode volume is proved to be power-related, and that of low-frequency modulation in the entire microresonator body turns out to be limited by the slow thermal relaxation rate. These results are verified experimentally in silica microspherical resonators. Such knowledge could facilitate RI control within WGM microresonators in applications of all-optical devices, e.g., nonlinear frequency conversion processes and tunable optical switching devices. In addition, the response function

Table 1. Parameters Used in the Fittings

g_{th} [Hz/K]	Γ_{abs} [Hz]	C_{sp} [J/(Kg K)]	κ_2 [W/(m K)]	ρ [Kg/m^3]
-1.6×10^9	9.5×10^3	740	0.026	2200
δR [μm]	D [m^2 s^{-1}]	K_2 [W/K]	C_2 [J/K]	β [MHz/mW]
1.4	8×10^{-7}	1.21×10^{-5}	3.45×10^{-7}	5

figure indicates new methods to estimate thermal constants of a microresonator.

APPENDIX A: SOLVING THE COUPLED EQUATIONS IN PERTURBATION APPROACH

In this section, we detail the process to determine the resonance frequency shift response functions $K(\Omega)$ and laser-microresonator relative frequency response function $R(\Omega)$ by solving the coupled Eqs. (1)–(3) using a perturbation approach.

When the pump wavelength scans in a small range, small signal quantities are introduced as Eqs. (A1)–(A4):

$$\alpha = \alpha_0 + \alpha_1(t). \tag{A1}$$

$$\Delta T_1 = \Delta T_1^0 + \Delta T_1^1(t). \tag{A2}$$

$$\Delta T_2 = \Delta T_2^0 + \Delta T_2^1(t). \tag{A3}$$

$$\Delta = \Delta_0 + \Delta_1(t). \tag{A4}$$

Here, α_0, Δ_0, ΔT_1^0, and ΔT_2^0 denote the steady-state intracavity field amplitude, laser-microresonator frequency detuning, and temperature differences between the mode volume (resonator body) and resonator body (the surroundings), respectively. For the modulation frequency of interest is much slower than the resonance bandwidth, the frequency detuning variable is time-dependent in Eq. (A4). By substituting Eqs. (A1)–(A4) into Eqs. (1)–(3), the solutions for steady-state operation are derived:

$$\alpha_0 = \frac{\sqrt{\kappa_{ex}}s}{\kappa/2 - i(\Delta - ig_{th}\Delta T_1^0(1 + k_2/k_1))}. \tag{A5}$$

$$\Delta T_1^0 = \frac{\Gamma_{abs}}{k_1}|\alpha_0|^2. \tag{A6}$$

$$\Delta T_2^0 = \frac{\Gamma_{abs}}{k_2}|\alpha_0|^2. \tag{A7}$$

And the time-dependent coupled equations describing the perturbation terms are achieved as

$$\begin{aligned}\dot{\alpha_1}(t) = &[i\Delta_1(t) - ig_{th}(\Delta T_1^1(t) + \Delta T_2^1(t))]\cdot\alpha_0 \\ &+ [i\Delta_0 - ig_{th}(\Delta T_1^0 + \Delta T_2^0) - \kappa/2]\cdot\alpha_1(t).\end{aligned} \tag{A8}$$

$$\dot{\Delta T_1^1}(t) = -\frac{k_1}{C_{p1}}\Delta T_1^1(t) + \frac{\Gamma_{abs}}{C_{p1}}[\alpha_0\alpha_1^*(t) + \alpha_0^*\alpha_1(t)]. \tag{A9}$$

$$\dot{\Delta T_2^1}(t) = \frac{k_1}{C_{p2}}\Delta T_1^1(t) - \frac{k_2}{C_{p2}}\Delta T_2^1(t). \tag{A10}$$

Because the cavity field damping rate is typically much faster than the thermal relaxation rate of the cavity, the steady-state solution of Eq. (A8) is used throughout the analysis:

$$\alpha_1 = \frac{i[\Delta_1(t) - g_{th}(\Delta T_1^1(t) + \Delta T_2^1(t))]\cdot\alpha_0}{\kappa/2 - i[\Delta_0 - g_{th}(\Delta T_1^0 + \Delta T_2^1)]}. \tag{A11}$$

By substituting Eq. (A11) into Eqs. (A9) and (A10) and performing Fourier transform of the results, the temperature changes both in the mode volume and the resonator body are related to the pump light wavelength detuning Δ_1:

$$\Delta\tilde{T}_1^1(\Omega) = K(\Omega)\cdot\tilde{\Delta}_1(\Omega). \tag{A12}$$

$$\Delta\tilde{T}_2^1(\Omega) = \frac{k_1/C_{p2}}{k_2/C_{p2} + i\Omega}K(\Omega)\cdot\tilde{\Delta}_1(\Omega). \tag{A13}$$

Here, Ω denotes the modulation frequency:

$$K(\Omega) = \frac{\beta\cdot P_{in}/g_{th}}{i\Omega + \frac{k_1}{C_{p1}} + \beta\cdot P_{in} + \beta\cdot P_{in}\frac{k_1}{C_{p2}}/\left(\frac{k_2}{C_{p2}} + i\Omega\right)}. \tag{A14}$$

$$\beta = g_{th}\frac{\Gamma_{abs}}{C_{p1}}\frac{2\kappa_{ex}(\Delta_0 - g_{th}\Delta T_0)}{\left[(\Delta_0 - g_{th}\Delta T_0)^2 + \frac{\kappa^2}{4}\right]^2}. \tag{A15}$$

Thus, we get the resonance frequency shift response function of the mode volume, $K_1(\Omega)$, and that of the microresonator body, $K_2(\Omega)$, as following:

$$K_1(\Omega) = \left(1 + \frac{k_1/C_{p2}}{k_2/C_{p2} + i\Omega}\right)\cdot g_{th}K(\Omega). \tag{A16}$$

$$K_2(\Omega) = \frac{k_1/C_{p2}}{k_2/C_{p2} + i\Omega}\cdot g_{th}K(\Omega). \tag{A17}$$

And the laser-microresonator relative frequency change for the mode volume is

$$\begin{aligned}\tilde{\Delta}_1^{lr}(\Omega) &= \tilde{\Delta}_1(\Omega) - g_{th}[\Delta\tilde{T}_1^1(\Omega) + \Delta\tilde{T}_2^1(\Omega)] \\ &= [1 - K_1(\Omega)]\cdot\tilde{\Delta}_1(\Omega).\end{aligned} \tag{A18}$$

For the resonator body, it is

$$\tilde{\Delta}_2^{lr}(\Omega) = \tilde{\Delta}_1(\Omega) - g_{th}\cdot\Delta\tilde{T}_2^1(\Omega) = [1 - K_2(\Omega)]\cdot\tilde{\Delta}_1(\Omega). \tag{A19}$$

Then the laser-microresonator relative frequency change response function $R_i(\Omega)$ takes the form of $1 - K_i(\Omega)(i = 1, 2)$.

Funding. Instrument Developing Project of the Chinese Academy of Sciences (YZ201353); National Natural Science Foundation of China (NSFC) (51205381, 61271139); The National High Technology Research and Development Program of China (2015AA042402).

Acknowledgment. We appreciate useful discussions with Jiabin Wu in CIOMP, and insightful instructions from Tal. Carmon in Israel Institute of Technology, Israel.

REFERENCES

1. K. J. Vahala, "Optical microcavities," Nature **424**, 839–846 (2003).
2. Y. C. Li, O. V. Svitelskiy, A. V. Maslov, D. Carnegie, E. Rafailov, and V. N. Astratov, "Giant resonant light forces in microspherical photonics," Light Sci. Appl. **2**, e64 (2013).
3. T. J. Kippenberg, S. M. Spillane, and K. J. Vahala, "Kerr-nonlinearity optical parametric oscillation in an ultrahigh-*Q* toroid microcavity," Phys. Rev. Lett. **93**, 083904 (2004).
4. M. Aspelmeyer, T. J. Kippenberg, and F. Marquardt, *Cavity Optomechanics-Nano- and Micromechanical Resonators Interacting with Light* (Springer, 2014).

5. K. H. Kim, G. Bahl, W. Lee, J. Liu, M. Tomes, X. D. Fan, and T. Carmon, "Cavity optomechanics on a microfluidic resonator with water and viscous liquids," Light Sci. Appl. **2**, e110 (2013).
6. V. S. Ilchenko and M. L. Gorodetskii, "Thermal nonlinear effects in optical whispering gallery microresonators," Laser Phys. **2**, 1004–1009 (1992).
7. T. Carmon, L. Yang, and K. J. Vahala, "Dynamical thermal behaviour and thermal self-stability of microcavities," Opt. Express **12**, 4742–4750 (2004).
8. S. Soltani and A. M. Armani, "Optothermal transport behavior in whispering gallery mode optical cavities," Appl. Phys. Lett. **105**, 051111 (2014).
9. D. Faenesi, A. Barucci, G. C. Righini, S. Berneschi, S. Soria, and G. N. Conti, "Optical frequency conversion in silica-whispering-gallery-mode microspherical resonators," Phys. Rev. Lett. **112**, 093901 (2014).
10. Q. Lin, J. Rosenberg, X. Jiang, K. J. Vahala, and O. Painter, "Mechanical oscillation and cooling actuated by the optical gradient force," Phys. Rev. Lett. **103**, 103601 (2009).
11. T. Herr, V. Brasch, J. D. Jost, C. Y. Wang, N. M. Kondratiev, M. L. Gorodetsky, and T. J. Kippenberg, "Temporal solitons in optical microresonators," Nat. Photonics **8**, 145–152 (2013).
12. C. Y. Qiu, J. Shu, Z. Li, X. Z. Zhang, and Q. F. Xu, "Wavelength tracking with thermally controlled silicon resonators," Opt. Express **19**, 5143–5148 (2011).
13. N. Vukovic, N. Healy, P. Mehta, T. D. Day, P. J. A. Sazio, J. V. Badding, and A. C. Peacock, "Thermal nonlinearity in silicon microcylinderical resonators," Appl. Phys. Lett. **100**, 181101 (2012).
14. W. S. Fegadolli, L. Feng, M. Mujeeb-U-Rahman, J. B. Oliveria, V. Almeida, and A. Scherer, "Experimental demonstration of a reconfiguration silicon thermo-optical device based on spectral tuning of ring resonators for optical signal processing," Opt. Express **22**, 3425–3431 (2014).
15. L. Fan, J. Wang, L. T. Varghese, H. Shen, B. Niu, Y. Xuan, A. M. Weiner, and M. H. Qi, "An all-silicon passive optical diode," Science **335**, 447–450 (2012).
16. J. Wang, L. T. Varghese, L. Fan, P.-H. Wang, Y. Xuan, D. E. Leaird, A. M. Weiner, and M. H. Qi, "One-way transmission of 10 Gbps data through a silicon optical diode based on nonreciprocal resonance reshaping," Opt. Express **22**, 25739–25745 (2014).
17. M. Agarwal and I. Teraoka, "All-photonic, dynamic control of optical path length in a silica sphere resonator," Opt. Lett. **38**, 2640–2643 (2013).
18. Q. L. Wang, Y. Wang, Z. Guo, J. F. Wu, and Y. H. Wu, "Thermal oscillatory behavior analysis and dynamic modulation of refractive index in microspherical resonator," Opt. Lett. **40**, 1607–1610 (2015).
19. J. Li, S. Diddams, and K. J. Vahala, "Pump frequency noise coupling into a microcavity by thermo-optic locking," Opt. Express **22**, 14559–14567 (2014).
20. I. Teraoka, "Analysis of thermal stabilization of whispering gallery mode resonance," Opt. Commun. **310**, 212–216 (2014).
21. H. Rokhsari and K. J. Vahala, "Observation of Kerr nonlinearity in microcavities at room temperature," Opt. Lett. **30**, 427–429 (2005).